

# DEFECT AND STRAIN TOLERANCE OF GIRTH WELDS IN HIGH STRENGTH PIPELINES

J. R. Gordon<sup>1</sup>, Gary Keith<sup>1</sup> and N.C. Gordon<sup>2</sup>

<sup>1</sup>Microalloying International, Inc.  
9977 W Sam Houston Parkway N, Suite 140; Houston, TX 77064; USA  
<sup>2</sup>Texas Tech University, Lubbock, Texas, USA

Keywords: Pipelines, ECA, Strain, Strain-based Design, Crack Driving Force, Pressure, Bi-axial Loading

## Abstract

Over the last 10 years a number of research programs have been performed to assess the behavior of pipeline girth welds under strain based loading and develop strain based Engineering Critical Analysis/Assessment (ECA) methods. These studies have highlighted that pressure-induced biaxial loading can have a significant influence on the strain capacity of girth welds. The major effect of biaxial loading is an increase in the crack driving force. In comparison, the material's resistance to fracture appears to be similar under uniaxial and biaxial loading. In North America strain based ECA models have recently been developed by ExxonMobil and Center for Reliable Energy Systems (CRES). This paper presents a comparison of these strain based ECA models and also compares the predictions from these models with the DNV RP 108 ECA procedure developed to assess pipelines installed by reeling.

## Introduction

The majority of existing pipeline design codes are stress based and provide limited guidance on the design and assessment of pipelines that may experience high strains during installation or operation. Although onshore pipelines generally do not experience high strains during installation, offshore pipelines installed by reeling are subjected to plastic strain cycles during installation (reeling on and reeling off). High strains can also occur in operating pipelines due to lateral or upheaval buckling, thaw settlement, frost heave, ground movement and seismic loading. In such cases pipelines should be designed based on strain capacity. However, strain based design poses a number of challenges, especially as related to pipeline girth welds and general material behavior. In addition, it is important that the existing Engineering Critical Assessment (ECA) methods developed for stress based loading are extended to cover strain based loading so that the significance of flaws can be assessed under high strain loading and appropriate flaw acceptance criteria can be established.

Over the last 10 years a number of research programs have been performed to assess the behavior of pipeline girth welds under strain based loading and to develop strain based ECA methods. These studies have highlighted that pressure-induced biaxial loading can have a significant influence on the strain capacity of girth welds. The major effect of biaxial loading is an increase in the crack driving force. In comparison, the material's resistance to fracture appears to be similar under uniaxial and biaxial loading.

Although DNV RP F108 [1] provides an industry accepted strain based ECA procedure for pipelines installed by reeling, until recently there were no strain based ECA models that could be used to evaluate pipelines that may experience high strains in operation. In North America strain based ECA models have recently been developed by ExxonMobil [2] and Center for Reliable Energy Systems (CRES) [3]. This paper presents a comparison of these strain based ECA models and also compares the predictions from these models with the DNV RP 108 ECA procedure developed to assess pipelines installed by reeling.

### **ECA Considerations for Strain Based Design**

#### General

When a fracture assessment is performed the applied crack driving force (derived from a fracture mechanics model) is compared to the materials resistance to fracture (material fracture toughness measured in the Test Laboratory). Fracture or plastic collapse is deemed to occur when the crack driving force or net section stress (Demand) exceeds the materials resistance to fracture or the material flow strength (Capacity). When developing strain based ECA models for pipelines that may experience high strains in operation it is important to account for the effect of pressure induced biaxial loading effects on both the crack driving force and the material's resistance to fracture and plastic collapse.

#### Effect of Biaxial Loading on Crack Driving Force

Gordon et al. performed a finite element analysis (FEA) study [4] to determine the effect of biaxial loading on the crack driving force of surface flaws in pipeline girth welds.

The nominal pipe and flaw details assumed in the FEA study can be summarized as follows:

- Pipe grade: API 5L X80
- Pipe diameter: 762 mm
- Wall thickness: 15.6 mm
- Flaw geometry:  $3 \times 50$  mm internal surface flaw
- Flaw locations: Parent pipe, weld center line (C/L), and fusion line.

The FEA matrix included the following variables:

- Welding process: SAW and GMAW-P
- Hoop stress: 0-80% specified minimum yield stress (SMYS)
- Axial loading: Tension and global bending
- HAZ softening: 0-10% Heat-Affected Zone (HAZ) softening
- Weld mismatch: 0, 15, and 30% overmatching of weld metal strength
- Pipe tensile properties: Isotropic and anisotropic
- Parent pipe Y/T ratio: Medium and high.

The stress strain curves used in the FEA models were based on measured stress strain curves obtained during parent pipe and weld procedure qualification testing. Full details of the FEA matrix and the material properties are presented in Reference [4].

The loading sequence adopted in the models with internal pressure was always to apply internal pressure first, with the end cap load not restrained, and then apply the axial loading. The pipeline strain was determined directly from the FEA model remote from the girth weld region. The strain was determined at 0, 90, 180, and 270 degree intervals around the pipe with 0 degree corresponding to the flaw centerline. The requirement for nominal strain measurement was to ensure that the model was long enough so that the axial strain variation at the ends of the model around the circumference was less than 1%.

Prior to performing finite element analyses of pipeline girth welds a series of baseline analyses was performed on parent pipe models to determine the effect of biaxial loading on applied CTOD without the complication of a girth weld and the added difficulties of accounting for weld metal mismatch and HAZ softening etc. Baseline analyses were performed for the following cases:

- Case 1: Identical tensile properties in the axial, hoop and through thickness directions, i.e., the measured hoop tensile stress strain curve was assumed for all three directions.
- Case 2: Actual tensile properties in the hoop and axial directions with the through thickness properties set equal to the axial tensile properties.

The results of the baseline analyses to determine the effect of internal pressure (hoop stress = 80% SMYS) on the crack driving force in parent pipe are summarized in Figure 1 as a plot of applied CTOD versus remote strain. It can be seen that as the remote strain increases the effect of internal pressure is to increase the applied crack driving force (CDF) as compared to zero internal pressure.

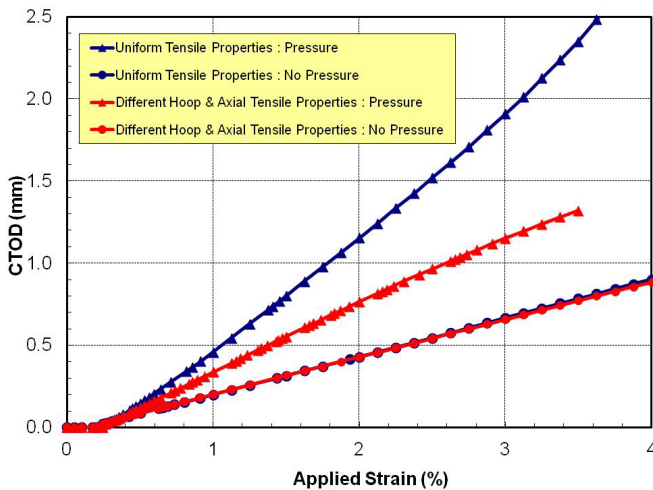


Figure 1. Effect of internal pressure on crack driving force [4].

The effect of internal pressure can be captured by a Biaxial Factor that compares the applied CTOD with internal pressure to the corresponding CTOD without internal pressure:

$$\text{CDF Biaxial Factor} = \frac{\text{CTOD}_{\text{Pressure}}}{\text{CTOD}_{\text{NO Pressure}}} \quad (1)$$

The FEA results presented in Figure 1 are re-plotted in Figure 2 in terms of the CDF Biaxial Factor. The results indicate that for remote strains less than the material yield strain (0.50%) the applied CTOD is not influenced by biaxial loading (i.e., the CDF Biaxial Factor = 1) but as the remote strain increases beyond the material yield strain the CDF Biaxial Factor increases until it reaches a plateau beyond which the CDF Biaxial Factor remains reasonably constant. For the two cases analyzed the steady state CDF Biaxial Factors were as follows:

- Case 1 (Uniform Tensile Properties) : CDF Biaxial Factor = 2.8
- Case 2 (Different Hoop & Axial Tensile Properties) : CDF Biaxial Factor = 1.8

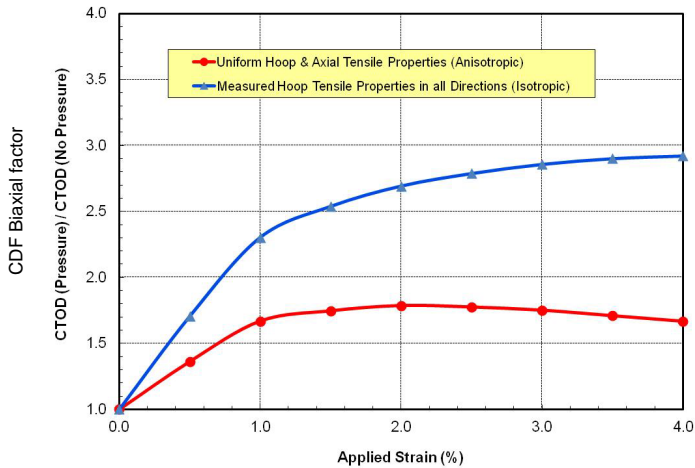


Figure 2. Variation in CDF Biaxial Factor with applied strain.

As you may expect the CDF Biaxial Factor is dependent on a number of variables including material tensile properties, applied strain, weld metal mismatch, HAZ softening, flaw location, Hi-Lo misalignment etc. Nevertheless, the FEA results indicated that the plateau values of the CDF Biaxial Factor ranges from 1.8 to 2.8 depending on the combination of variables with an average value of approximately 2.0, i.e. on average the effect of internal pressure is to increase the applied crack driving force by a factor of approximately 2.0 under strain based loading.

### Effect of Biaxial Loading on Resistance to Fracture

The standard fracture toughness specimen geometry for ECA analysis is the Single Edge Notch Bend (SENB) specimen. This specimen geometry, which is loaded in three point bending, provides a high level of constraint and, as a result, produces conservative toughness values. Although the SENB specimen geometry is the default specimen geometry for normal ECAs the use of Single Edge Notch Tension (SENT) specimens has become increasingly common for pipeline ECAs since the level of constraint in a SENT specimen is much more similar to the constraint in a pipeline girth weld. It should be noted that even if a pipeline experiences global bending the through wall stress distribution at a specific location (e.g., 12 o'clock) is predominantly membrane with only a small through wall thickness stress variation.

ExxonMobil [5] has conducted an extensive experimental program with supporting numerical analysis to characterize the fracture behavior of parent pipe and pipeline girth welds under uniaxial and biaxial loading. The experimental test matrix included parent pipe samples and girth welded pipe samples fabricated from DSAW and seamless pipe (API 5L Grades X60 – X80). The experimental test program included the following fracture tests:

- Single Edge Notch Bend (SENB) Tests
- Single Edge Notch Tension (SENT) Tests
- Curved Wide Plate (CWP) Tests
- Full Scale Pressurized Pipe (FSPP) Tests.

The results of the fracture tests were analyzed to generate CTOD R-curves in which the measured CTOD (derived from a double clip gauge arrangement) was plotted against slow stable crack growth. The results of the fracture tests are summarized in Figures 3 and 4.

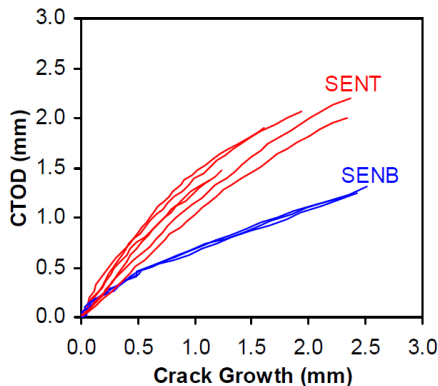


Figure 3. Comparison of SENB and SENT CTOD R-Curves [5].

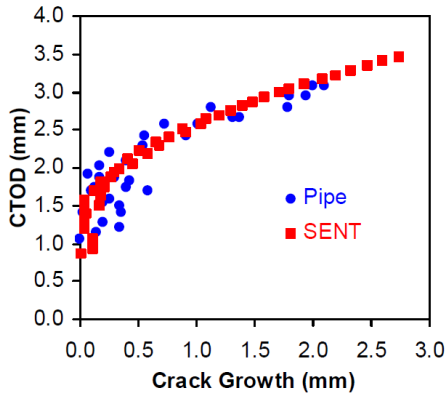


Figure 4. Comparison of SENT and full scale pressurized pipe CTOD R-curves [5].

Figure 3 compares the CTOD R-curves obtained from highly constrained SENB specimens with corresponding CTOD R-curves obtained from low constraint SENT specimens. The results clearly illustrate the lower constraint SENT specimen produces a much steeper R-curve, i.e., the measured resistance to ductile tearing is much higher in a SENT test as opposed to the highly constrained SENB test. Figure 4 compares the CTOD R-curves obtained from SENT and FSPP tests. It can be seen that the SENT CTOD R-curve is nominally identical to the CTOD R-curve obtained from the Full Scale Pressurized Pipe test confirming that the resistance to tearing is the same under uniaxial and biaxial loading, i.e., pressure loading does not influence resistance to tearing.

#### Effect of Biaxial Loading on Plastic Collapse

Although the yield strength of a material is generally measured by performing a simple uniaxial tensile test, yielding is a three dimensional phenomenon. There are a number of yield criteria which consider a three dimensional stress state. The Von Mises criterion is probably the most widely used method of defining an equivalent stress or defining the stress state that will result in material yielding,

The Von Mises equivalent stress is defined as follows:

$$\sigma_{VM} = \left\{ \frac{1}{2} \left[ (\sigma_1 - \sigma_2)^2 + (\sigma_1 - \sigma_3)^2 + (\sigma_2 - \sigma_3)^2 \right] \right\}^{0.5} \quad (2)$$

where  $\sigma_1$ ,  $\sigma_2$  and  $\sigma_3$  are the principal stresses in all three directions.

Yielding is predicted to occur when the Equivalent Stress equals the material uniaxial yield strength. In the case of a pipe that is under internal pressure and subjected to axial loading (i.e., a biaxial stress state since the through wall stress can be ignored for thin wall pipes) Equation 2 predicts that yielding will occur when the axial stress ( $\sigma_L$ ) achieves the following value:

$$\sigma_L = \frac{\sigma_H}{2} + \left[ \sigma_{YS}^2 - \frac{3}{4} \sigma_H^2 \right]^{1/2} \quad (3)$$

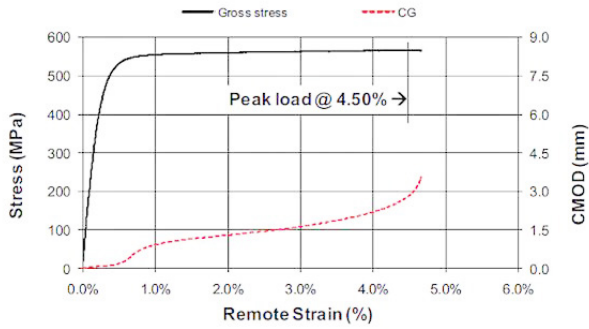
Where:         $\sigma_{YS}$     = Uniaxial Yield Strength  
                    $\sigma_H$      = Hoop Stress

For a pipeline operating at a Hoop Stress equal to 72% of the material yield strength Equation (3) predicts that yielding will occur when the Axial Stress equals 1.14 times the uniaxial yield strength. Consequently, pipelines operating under internal pressure will exhibit a higher yield strength than the uniaxial yield strength. This is illustrated in Figure 5 which presents the applied stress vs. displacement records for the following tests performed as part of a Pipeline Research Council International/US Department of Transportation (PRCI/DOT) funded Research Project [6].

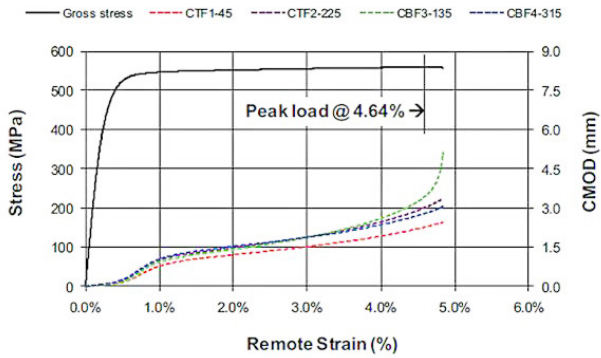
Curved Wide Plate Test  
 Full Scale Pipe Test : No Internal Pressure  
 Full Scale Pipe Test : Internal Pressure

The tests were all performed on nominally identical girth welded samples with surface flaws that were the same size.

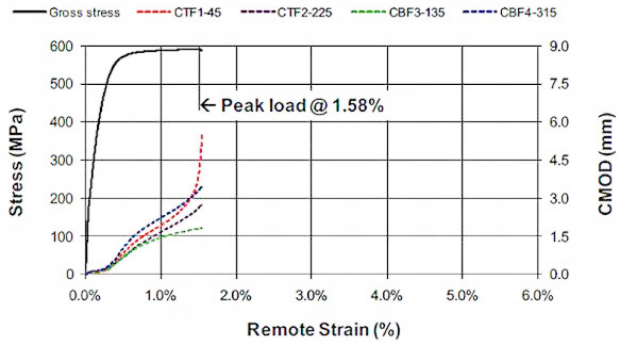
The results in Figure 5 clearly highlight that the Full Scale Pipe Test with internal pressure (Figure 5c) has a yield strength that is approximately 15% higher than the unpressurized Full Scale Tests and the Curved Wide Plate Test (Figures 5a & 5b). Figure 5 also confirms that beyond yield the load displacement records for the pressurized and unpressurized samples follow the same general trend with test records that remain essentially parallel to each other, i.e., not only is yielding increased by around 15% but so is the material tensile strength. The increase in material yield strength and tensile strength will result in an increase in the plastic collapse stress for the pressurized pipe. Although the effect of biaxial loading on plastic collapse can be accounted for in an ECA by increasing the apparent yield and tensile strength of the pipe material to account for biaxial loading this simple correction does not account for the increase in Crack Driving Force produced under biaxial loading at strain levels in excess of yield.



a) Curved Wide Plate (Specimen 3.1b)



b) Pipe – Effectively No Pressure (Specimen 1.6)



c) Pipe – High Pressure (Specimen 1.5)

Figure 5. Comparison of curved wide plate, unpressurized pipe and pressurized pipe load vs. displacement records [6]. CMOD – Crack Mouth Opening Displacement.

### Strain Based ECA Models

#### General

Over the last few years several strain based ECA procedures have been developed:

- DNV RP F108 Strain Based ECA procedures for Pipelines installed by Reeling
- ExxonMobil Strain Based ECA Model
- Center for Reliable Energy Systems (CRES) Strain Based ECA Model.

Although all three models have similarities they also have fundamental differences.

#### DNV RP F108

In 2006 DNV published DNV RP 108 which includes an ECA procedure for pipelines that experience plastic strain cycles during installation, i.e. pipelines that are installed by reeling. Although the ECA procedures in DNV RP F108 assess reeling strains well beyond yield (e.g. reeling strains ~ 2.0% per cycle are not uncommon) the ECA procedures in DNV RP F108 are based on the BS 7910 [7] approach which is a stress based ECA methodology. This requires that the installation strain history is converted into an equivalent stress history.

DNV RP F108 includes procedures to convert the strain history into an equivalent stress history using the material stress-strain curve. Since girth welds in reeled pipe are required to overmatch the base parent pipe tensile properties the parent pipe stress strain curve is used to determine an equivalent stress that corresponds to the maximum strain the pipe will experience during reeling on and reeling off. For the first reel cycle the parent pipe stress strain curve in the “As-Received” condition is used. For the second and subsequent reel cycles the parent pipe stress strain curve in the “Strained” condition is used to account for the Bauschinger effect in prior reel

cycles. Only the tensile component of each straining cycle is considered to contribute to fracture. Both the 6 o'clock and 12 o'clock positions are considered unless the strain cycles are sufficiently similar that they may be considered to be equivalent. The maximum positive and negative strains for each half cycle throughout installation are assumed to lie on the same plane, i.e. it is assumed that there is no pipe rotation during reeling.

Although DNV RP F108 does not require local weld toe ( $M_k$ ) effects to be considered for applied strains  $> 0.40\%$  it does require consideration of Hi-Lo misalignment. DNV RP F108 includes a procedure to account for girth weld Hi-Lo misalignment using the Neuber method as outlined below.

### Step 1: Calculate the Stress Concentration Factor due to Misalignment

The Stress Magnification Factor ( $K_t$ ) due to axial misalignment is calculated using the following equation:

$$K_t = 1 + \frac{6\delta}{T_1} \left[ \frac{1}{1 + \left(\frac{T_2}{T_1}\right)^\beta} \right] e^{-\alpha} \quad (4)$$

$$\alpha = \frac{1.82L}{\sqrt{(DT_1)}} \cdot \frac{1}{\left[ 1 + \left(\frac{T_2}{T_1}\right)^\beta \right]} \quad (5)$$

$$\beta = 1.5 - \frac{1.0}{\text{Log}\left(\frac{D}{t}\right)} + \frac{3.0}{\left[\text{Log}\left(\frac{D}{t}\right)\right]^2} \quad (6)$$

where:

$\delta$	=	centerline eccentricity ( $\delta = \text{Hi-Lo} + 0.5 \cdot (T_1 - T_2)$ )
Hi-Lo	=	Internal Hi-Lo misalignment
$T_1$	=	the thickness of the thicker pipe
$T_2$	=	the thickness of the thinner pipe
$L$	=	width of weld

### Step 2: Develop a Neuber Curve

The Neuber equation is as follows:

$$\sigma_{actual}\epsilon_{actual} = \sigma_{nominal}\epsilon_{nominal}K_t^2 \quad (7)$$

where:	$\sigma_{actual}$	=	actual stress (including SCF)
	$\epsilon_{actual}$	=	actual strain (including SCF)
	$\sigma_{nominal}$	=	nominal stress (excluding SCF)
	$\epsilon_{nominal}$	=	nominal strain (excluding SCF)
	$K_t$	=	elastic stress concentration factor (SCF)

### Step 3: Determine the Equivalent Stress

The Equivalent Stress is determined as the intersection point between the Neuber curve ( $\sigma_{nominal}\epsilon_{nominal}K_t^2/\sigma_{actual}$  plotted against  $\sigma_{nominal}$ ) and the appropriate parent pipe axial stress-strain curve.

### Step 4: Partition the Equivalent Stress into Membrane and Bending Components

The Equivalent stress determined from Step 3 is partitioned into membrane ( $P_m$ ) and local through wall bending ( $P_b$ ) stresses as follows:

- $P_m$  = Nominal Stress corresponding to nominal reeling strain derived from parent pipe stress strain curve.
- $P_b$  = Additional stress component associated with Hi-Lo misalignment (i.e. the difference between the Equivalent Stress determined in Step 3 and  $P_m$ ).

This is standard practice and is justified on the basis that misalignment at welded joints produces secondary bending across the welded joint. Although the misalignment stresses are referred to as secondary stresses (i.e. they are a consequence of misalignment rather than applied loading) they do contribute to plastic collapse and as a result from an ECA perspective they should be treated as primary bending stresses.

Since reeling is strain controlled DNV RP F108 permits the  $L_r$  cut-off in the Failure Assessment Diagram (FAD) to be extended. The Installation ECA can use the following  $L_r$  max cut-off:

$$L_{r\max} = \frac{\sigma_{TS}}{\sigma_{YS}} \quad (8)$$

where	$\sigma_{TS}$	=	Material Tensile Strength
	$\sigma_{YS}$	=	Material Yield Strength

ECA analyses are performed for each reeling cycle using the Level 3B FAD based procedure in BS 7910 to predict the stable crack growth in each reeling event. The material toughness is defined as the lowest JR-curve derived from SENT specimens notched into both the girth weld

and HAZ. The material stress–strain curve used in the ECA analysis is the parent pipe axial stress strain curve, i.e. no credit is taken for weld metal overmatch. DNV RP F108 recommends that the total stable crack growth during installation should be limited to 1.0 mm.

Although the objective of DNV RP F108 is to determine the extent of stable crack growth during reel installation the same procedure can be used to determine limiting flaw sizes for pipelines that experience a single strain event. It should be noted however that DNV RP F108 does not consider the effect of biaxial loading on plastic collapse or Crack Driving Force. Also, as noted above it, does not take into account weld metal overmatch.

#### ExxonMobil Strain Based ECA Model

ExxonMobil has developed a multiple tier framework to predict the tensile strain capacity of pipeline girth welds that contain flaws or determine flaw acceptance criteria for a given target strain. Through finite element analyses (FEA) or simplified equations, strain capacity is predicted based on input parameters such as pipe geometry, internal pressure, material properties, girth weld defect size, and Hi-Lo misalignment.

A 3 Tier methodology has been proposed to enable girth welds to be assessed at a level of complexity appropriate to the application under consideration. The Level 1 and 2 procedures use parametric equations that enable direct calculation of tensile strain capacity. At Level 1 several of the input parameters are fixed to simplify the equations and introduce an added margin of safety. The Level 2 parametric equations provide the user the option of assessing a broader range of input parameters to help optimize tensile strain capacity and develop more representative girth weld flaw acceptance criteria. The Level 3 procedure is the most complicated and accurate method of assessing tensile strain capacity but requires Project specific testing in combination with detailed finite element analysis. Although the Level 3 method may be used for critical applications, where for example the tensile strain demand is high, the Level 1 and 2 procedures provide the user with tools to evaluate preliminary designs and develop provisional flaw acceptance criteria.

The ExxonMobil models are based on a Crack Driving Force/R-Curve approach where the limiting condition is defined as the applied strain which produces a crack driving force curve that is tangential to the R-curve as illustrated in Figure 6. In the schematic in Figure 6 the material R-curve is assessed against a series of crack driving force curves corresponding to different remote strains ( $\epsilon_1$ ,  $\epsilon_2$ ,  $\epsilon_3$  and  $\epsilon_4$ ). The tangency condition is defined as point A on the Crack Driving Force Curve for an applied strain equal to  $\epsilon_3$ .

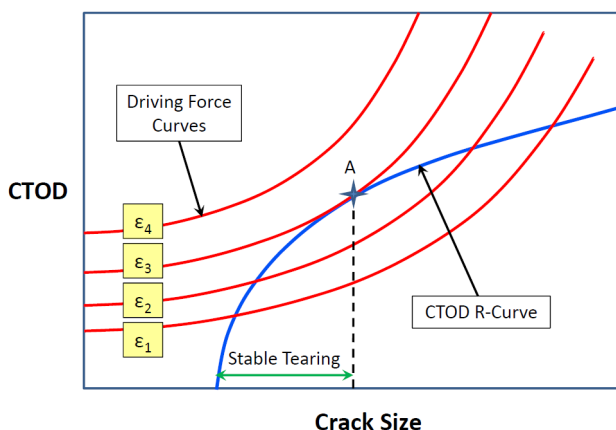


Figure 6. Crack Driving Force vs. R-curve schematic.

The Crack Driving Force/R-curve approach outlined in Figure 6 has been used to assess ductile fracture for over 25 years and is the approach adopted within the nuclear industry to assess ductile fracture. The novel feature of the ExxonMobil model is that instead of developing Crack Driving Force curves for constant values of stress the Crack Driving Force curves are derived for constant values of strain. Furthermore, whereas the Crack Driving Force/R-curve method is normally applied in cases where the applied stress is less than the material yield strength (i.e. the global response of the structure is elastic) the ExxonMobil model permits assessments to be performed under conditions of global yielding.

The R-curve used in the ExxonMobil model is a CTOD R-curve obtained from SENT specimens with crack depth to specimen width ( $a/W$ ) ratios that are larger than the maximum expected flaw size in operation or the target flaw acceptance criteria, i.e., the crack size in the SENT specimen is bigger than the proposed flaw acceptance criteria. SENT R-curve tests are performed on both weld metal and HAZ notched samples and the lowest R-curve is used in the assessment. For a Level 3 analysis the measured CTOD R-curve is used directly in the strain based ECA analysis where it is compared to the FEA predicted Crack Driving Force curves. At Level 2 the measured SENT R-curve is compared against three reference CTOD R-curves defined by ExxonMobil (Lower Bound, Average and Upper Bound) as shown in Figure 7. The reference R-curve that is closest to, but below, the measured R-curve is selected for the ECA analysis and the constants for that R-curve are used in the Level 2 parametric equations. For a Level 1 analysis the Lower Bound SENT CTOD R-curve in Figure 7 is assumed in the parametric equations.

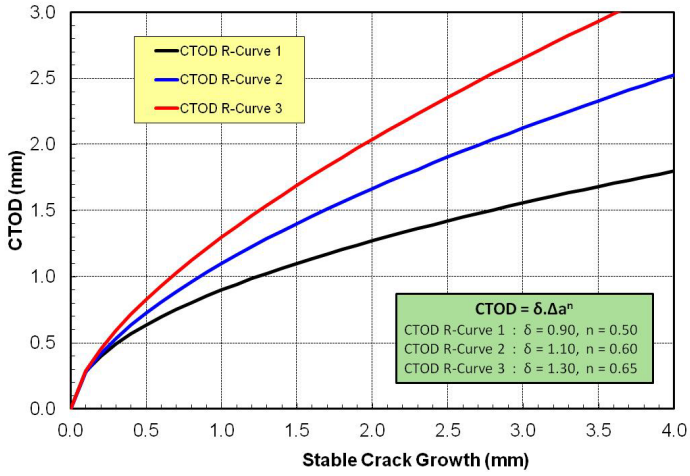


Figure 7. ExxonMobil CTOD R-curves.

The parametric equations for Levels 1 and 2 are as follows:

Level 1 (Grade X60 and X70)

$$\varepsilon_{C\_X60\_X70} = (.9 + .09\lambda) * \left[ \left\{ \alpha_1[C \cdot \lambda] + \alpha_2[C] + \alpha_3[\lambda] + \alpha_4 \right\} * \ln \left[ \frac{aC}{(t-a)^2} \right] + \left\{ \alpha_5[C \cdot \lambda] + \alpha_6[C] + \alpha_7[\lambda] + \alpha_8 \right\} \right] \quad (9)$$

Level 1 (Grade X80)

$$\varepsilon_{C\_X80} = \left\{ \beta_1[\lambda] + \beta_2 \right\} * \ln \left[ \frac{aC}{(t-a)^2} \right] + \left\{ \beta_3[\lambda] + \beta_4 \right\} \quad (10)$$

Level 2 (Grade X60 and X70)

$$\varepsilon_{C\_X60\_X70} = (9 + 0.0\lambda) * \left[ \begin{array}{l} \left\{ \begin{array}{l} x_1[C \cdot UEL \cdot \lambda \cdot e] + x_2[C \cdot \lambda \cdot e] + x_3[C \cdot UEL \cdot e] + x_4[C \cdot e] \\ + x_5[C \cdot UEL \cdot \lambda] + x_6[C \cdot \lambda] + x_7[C \cdot UEL] + x_8[C] \\ + x_9[UEL \cdot \lambda \cdot e] + x_{10}[\lambda \cdot e] + x_{11}[UEL \cdot e] + x_{12}[e] \\ + x_{13}[UEL \cdot \lambda] + x_{14}[\lambda] + x_{15}[UEL] + x_{16} \end{array} \right\} \\ * \ln \left[ \frac{aC}{(t-a)^2} \right] \\ + \left\{ \begin{array}{l} x_{17}[C \cdot UEL \cdot \lambda \cdot e] + x_{18}[C \cdot \lambda \cdot e] + x_{19}[C \cdot UEL \cdot e] + x_{20}[C \cdot e] \\ + x_{21}[C \cdot UEL \cdot \lambda] + x_{22}[C \cdot \lambda] + x_{23}[C \cdot UEL] + x_{24}[C] \\ + x_{25}[UEL \cdot \lambda \cdot e] + x_{26}[\lambda \cdot e] + x_{27}[UEL \cdot e] + x_{28}[e] \\ + x_{29}[UEL \cdot \lambda] + x_{30}[\lambda] + x_{31}[UEL] + x_{32} \end{array} \right\} \end{array} \right] \quad (11)$$

Level 2 (Grade X80)

$$\varepsilon_{C\_X80} = \left\{ \begin{array}{l} y_1[UEL \cdot \lambda \cdot e] + y_2[\lambda \cdot e] + y_3[UEL \cdot e] + y_4[e] \\ + y_5[UEL \cdot \lambda] + y_6[\lambda] + y_7[UEL] + y_8 \end{array} \right\} * \ln \left[ \frac{aC}{(t-a)^2} \right] + \left\{ \begin{array}{l} y_9[UEL \cdot \lambda \cdot e] + y_{10}[\lambda \cdot e] + y_{11}[UEL \cdot e] + y_{12}[e] \\ + y_{13}[UEL \cdot \lambda] + y_{14}[\lambda] + y_{15}[UEL] + y_{16} \end{array} \right\} \quad (12)$$

where

$\varepsilon_c$	=	Tensile Strain Capacity
$a$	=	Crack depth
$C$	=	Half Crack length
$\lambda$	=	Weld Metal Overmatch (based on Tensile Strength)
$UEL$	=	Uniform Strain to maximum Load in a Tensile Test
$\alpha, \beta$	=	Constants in Level 1 Equations
$x, y$	=	Constants in level 2 Equations

The Constants in the Level 1 and level 2 parametric equations are available in Reference 2.

Although the Level 2 Equations offer increased flexibility and allow the user to specify Hi-Lo misalignment, UEL and material toughness, the Level 1 and Level 2 equations include a number of simplifying assumptions as in Table I.

Table I. Simplifying Assumptions for Level 1 and Level 2 Equations

Parameter	Level 1	Level 2
Hi-Lo Misalignment	3.0 mm	Variable
Y/T Ratio	0.90	0.90
UEL (Uniform Strain)	6%	Variable
CTOD R-curve	Lower Bound (1)	Variable (1, 2 or 3)
Internal Pressure	80%	80%

The Level 1 and 2 parametric equations have the following validity limits:

Table II. Validity Limits for ExxonMobil Tensile Strain Capacity Equations

Parameter	Level 1		Level 2	
	X60-X70	X80	X60-X70	X80
Hi-Lo Misalignment	3.0 mm		0.0 - 3.0 mm	
UEL (Uniform Strain)	6%		6 - 12%	4.4 - 8%
Overmatch (%)	5 - 50%	5 - 20%	5 - 50%	5 - 20%
Flaw Height (mm)	2.0 - 5.0 mm		2.0 - 5.0 mm	
Flaw Length (mm)	20 - 50 mm		20 - 50 mm	

### CRES Strain Based ECA Model

CRES, C-FER and Microalloying International performed a joint project for Pipeline Research Council International (PRCI) and the US Department of Transportation (DOT) to develop and validate strain based design assessment methods for pipeline girth welds. The project included small and full scale experimental tests performed by Microalloying and C-Fer as well as detailed FEA analysis performed by CRES to develop a strain based ECA model.

CRES has proposed a Multi-Level (4 Tier) procedure to evaluate tensile strain capacity:

Level 1 – Initial Screening. The Level 1 model is intended for a quick estimation of the likely tensile strain capacity (TSC). The TSC is tabulated for selected pipe dimensions, material properties, and flaw size. The apparent toughness is estimated from upper shelf Charpy impact energy.

Level 2 – Normal Assessment (Standard Toughness Data). The Level 2 models are given in a library of parametric equations. The apparent toughness is estimated from either upper shelf Charpy impact energy or the upper shelf standard CTOD toughness.

Level 3 – Advanced Assessment (Low Constraint Toughness). The Level 3 models have two options. Level 3a uses an initiation control limit state. Level 3b uses a ductile instability limit state. In Level 3a, the TSC is given by the same library of parametric equations as in Level 2. The apparent toughness may be obtained by a number of low constraint test options. They include shallow-notched SENB, SENT, and CWP. In Level 3b, the crack driving force,  $CTOD_F$ , is expressed by a group of iso-strain curves constructed from the same library of parametric equations as Level 2. In this application, various levels of strain are given as a function of flaw

depth from the equations. The R-curve, often expressed in an equation form with two fitted parameters, is plotted on the same CTOD<sub>F</sub> vs. flaw depth chart. The R-curve may be obtained from small-scale low-constraint test specimens (e.g., shallow-notched SENB or SENT) or Curved Wide Plate tests.

Level 4 – Advanced Analysis with Direct FEA Calculation. The Level 4 models are structured in two options, similar to that of Level 3. In contrast to the Level 3 models, where the driving force relations are expressed in parametric equations, the driving force curves in Level 4 are directly obtained from FEA.

The strain based ECA models developed by CRES have two limit states: (1) initiation control and (2) ductile instability. Only the initiation controlled limit state is examined in this paper. The toughness in the initiation limit state is based on “apparent CTOD toughness” which is defined as the CTOD at the onset of stable crack growth in a low constraint fracture test. The apparent CTOD can be estimated as follows:

Apparent Toughness from Upper Shelf Charpy Energy. The apparent toughness ( $\delta_A$  in mm) may be obtained from the upper shelf Charpy energy (CVN in ft.lb) by the following equations up to an apparent CTOD of 1.2 mm:

$$CTOD_A = \left(0.0080 \cdot \frac{Y}{T} - 0.0014\right) \cdot CVN_{us} \text{ for X52 to X65, and} \quad (13)$$

$$CTOD_A = \left(0.0086 \cdot \frac{Y}{T} - 0.0021\right) \cdot CVN_{us} \text{ for X70 and X80,} \quad (14)$$

Apparent Toughness from Standard Deeply-Notched SENB. A multiplication factor of 1.5-2.0 may be applied to the upper-shelf CTOD toughness ( $\delta_m$ ) to obtain the apparent toughness. This conversion factor is applicable to standard CTOD specimens without side grooves. A default conversion factor of 1.75 is recommended.

Apparent Toughness from SENT Resistance Curves. The apparent toughness may be obtained from SENT CTOD R-curves at a flaw growth of 0.5-1.0 mm. The value of flaw growth, at which the apparent toughness is obtained, depends on pipe wall thickness and less so on other parameters. It is recommended that the amount of flaw growth, at which the apparent toughness is obtained, is linearly scaled between 0.5 mm for 12.7 mm (0.5 inch) wall thickness to 1.0 mm for 25.4 mm (1.0 inch) wall thickness.

Apparent Toughness from Shallow-Notched SENB Resistance Curves. The work by CANMET [8] has shown that R-curves obtained from shallow-notched SENB specimens are similar to those from SENT specimens, of the same material. Consequently, the same procedure for the SENT specimens may be applied to shallow-notched SENB specimens.

CRES has developed Tensile Strain Capacity (TSC<sub>p</sub>) equations for girth welds in pipe under internal pressure made with Gas Metal Arc Welding (GMAW) and either Shielded Metal Arc Welding (SMAW) or Flux Core Arc Welding (FCAW). The main reason for developing different equations for GMAW and SMAW/FCAW girth welds is the difference in weld geometry, since mechanized GMAW welds tend to be narrow with steep side walls (bevels) as opposed to SMAW and FCAW girth welds which are much wider with much shallower bevels.

The TSC prediction models consider the effects of the following parameters on girth weld strain capacity.

**Geometric Parameters**

- $t$  pipe wall thickness, mm,
- $a$  flaw height, mm,
- $2c$  flaw length, mm,
- $h$  girth weld high-low misalignment, mm.

**Material Parameters**

- $\sigma_y$  pipe yield strength, MPa,
- $\sigma_U$  pipe ultimate tensile strength, MPa,
- $\sigma_{UW}$  weld metal tensile strength, MPa,
- $\delta_A$  girth weld apparent CTOD toughness, mm.

**Loading Parameters**

- $P_f$  pressure factor, ratio of applied hoop stress to pipe yield strength.

The TSC equations are given as functions of the following normalized geometric and material parameters, apparent CTOD toughness and pressure factor:

- $H$  =  $a/t$  normalized flaw depth,
- $\beta$  =  $2c/t$  normalized flaw length,
- $\psi$  =  $h/t$  normalized girth weld high-low misalignment,
- $\xi$  =  $\sigma_y/\sigma_U$  base metal Y/T ratio,
- $\phi$  =  $\sigma_{UW}/\sigma_U$  weld metal strength mismatch ratio measured at ultimate tensile strength,
- $\delta_A$  girth weld apparent CTOD toughness, mm, and
- $P_f$  pressure factor, ratio of hoop stress to pipe yield strength.

The  $TSC_p$  equations for GMAW and FCAW / SMAW girth welds both have the following form:

$$TSC_p = A \frac{f(\delta_A)}{1 + f(\delta_A)}, \tag{15}$$

Where:

$$f(\delta_A) = (C\delta_A)^{B\delta_A^D}. \tag{16}$$

The terms  $A$ ,  $B$ ,  $C$ , and  $D$  in Equations 15 and 16 represent fitted functions of normalized geometry and material parameters. The Tensile Strain Capacity obtained using Equations 15 and 16 assumes a default pipe wall thickness of 15.9 mm and an internal pressure which produces a hoop stress in the range 60-80% of the pipe material SMYS. Correction factors are provided in

Reference [3] to enable TSC to be corrected for different pipe wall thicknesses and internal pressures.

Full details of the CRES Tensile Strain Capacity model and the equations are provided in Reference [3].

The applicable ranges of the input parameters of the TSC equations are as follows:

$\eta = a/t$	0.05 – 0.50
$\beta = 2c/t$	1.0 – 20.0
$\psi = h/t$	0.0 – 0.20
$\xi = \sigma_y/\sigma_U$	0.75 – 0.94
$\phi = \sigma_{UW} / \sigma_U$	1.0 – 1.3
$\delta_A$	0.0 – 2.5 mm
$P_f$	0.0 – 0.80

### Comparison of ExxonMobil and CRES Strain Based ECA Models

#### General

A series of sensitivity analyses was conducted using the ExxonMobil and CRES Tensile Strain Capacity models for the following pipeline application to compare the tensile strain capacity predictions:

- Pipe Grade                      API 5L X80
- Pipe Diameter                 36 inch
- Pipe Wall                        18.4 mm
- Flaw Geometry                 Surface Flaw
- Target Flaw Size               3 x 50 mm

The following base case parameters were assumed in the analysis:

- Material Toughness
  - ExxonMobil                   : ExxonMobil SENT CTOD R-curve 2
  - CRES                         :  $\delta_A$  derived from ExxonMobil SENT CTOD R-curve 2 at the recommended crack growth adjusted for thickness.
- Pipe Tensile Properties     : Specified Minimum
- Uniform Elongation         : 8%
- Weld Overmatch             : 20%
- Hi-Lo Misalignment         : 3.0 mm
- Hoop Stress                 : 80% SMYS

Sensitivity Analyses were performed for the following range of parameters:

- Material Toughness
  - ExxonMobil                   : CTOD R-curve 1, 2 and 3
  - CRES                         :  $\delta_A$  derived from appropriate SENT CTOD R-curve at the recommended crack growth adjusted for thickness.
- Uniform Elongation         : 4 – 10%
- Weld Overmatch             : 0 – 30%

- Hi-Lo Misalignment : 0.0 - 3.0 mm
- Hoop Stress : 50 - 80% SMYS

In the sensitivity analyses only one parameter was changed at a time, i.e. the remaining parameters were fixed at the base case values. The results of the sensitivity analyses are all plotted on the same vertical scale (Tensile Strain Capacity) to highlight the effect of the input parameters. The slope of the response curves gives an indication of how sensitive tensile strain capacity is to the input parameter, the steeper the response the more dependent tensile strain capacity is to the input parameter.

Results of Sensitivity Analyses

Material Toughness. The effect of material toughness on Tensile Strain Capacity is highlighted in Figure 8. It can be seen that all three sets of results (ExxonMobil and CRES GMAW and SMAW/FCAW) exhibit a similar trend with tensile strain capacity increasing with material toughness. The increase in Tensile Strain Capacity is approximately 0.2% from the lowest to the highest CTOD R-curve.

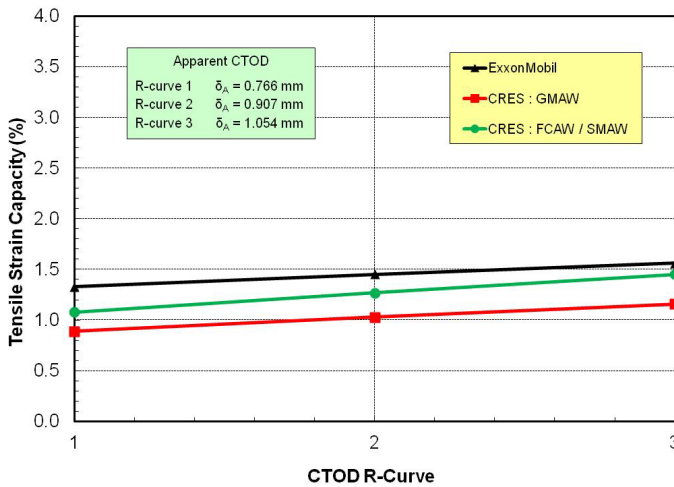


Figure 8. Effect of material CTOD toughness on tensile strain capacity.

In Figure 8 the apparent CTOD was determined from the SENT CTOD R-curve, i.e., the method of estimating apparent CTOD was consistent. However the CRES model permits apparent CTOD to be determined several different ways. During a recent Weld Procedure Qualification (WPQ) program Charpy, traditional CTOD and SENT R-curve tests were performed to fully characterize the mechanized girth weld. The test results were analyzed to determine how sensitive the apparent CTOD was to the method of estimating toughness. The calculated apparent CTOD values (calculated using the recommended procedures) and the associated Tensile Strain Capacities for the base case example are summarized below:

Table III. Apparent CTOD Estimates from a Single Weld Procedure Qualification

Test Method	Apparent CTOD (mm)	Tensile Strain Capacity (%)
Charpy	0.665	0.78
SENB CTOD	0.455	0.54
SENT CTOD R-curve	0.952	1.07

It can be seen that the calculated apparent toughness can vary significantly for a single weld procedure depending on the method of estimating apparent CTOD. The predicted tensile strain capacity for the apparent CTOD determined from the SENT R-curve is almost twice the tensile strain capacity determined using the apparent CTOD obtained from the standard SENB CTOD test. Indeed the variation in apparent CTOD from the different estimation methods and a single set of WPQ test results is larger than the variation between the ExxonMobil lower and upper bound SENT CTOD R-curves. These results highlight that the CRES Tensile Strain Capacity model may be more sensitive to the method of calculating apparent toughness than modest variations in toughness obtained using a consistent test method.

Although the different methods of deriving apparent CTOD toughness can produce different estimates of apparent CTOD toughness, the flexibility of being able to derive apparent CTOD toughness from Charpy or traditional CTOD test results can be useful in situations where SENT test data is not available, e.g., a pipeline that has already been installed and the Weld Procedure Qualification test program did not include SENT tests. The apparent CTOD toughness derived from traditional tests, i.e., Charpy and SENB, is more conservative than that from SENT. If the predicted strain capacity from traditional test data is sufficient, no further testing may be needed. This approach is consistent with multi-tier assessment procedures, such as BS 7910. The higher level approach may produce less conservative and accurate results at the expense of more elaborate testing.

The relative tensile strain capacities between the GMAW and SMAW/FCAW in Figure 8 appears to be surprising initially as GMAW welds are expected to have higher tensile strain capacity than SMAW/FCAW welds. The trend shown in Figure 8 is developed on the assumption that the SMAW/FCAW welds have the same toughness and have the same weld strength overmatch as the GMAW welds. Given the larger bevel and greater overmatched weld volume, the SMAW/FCAW welds have small crack driving force at the same weld strength mismatch level and flaw size. Actual SMAW/FCAW welds would generally have lower toughness and produce lower weld metal strength than GMAW welds. These differences will lead to lower tensile strain capacity of SMAW/FCAW welds than GMAW welds.

Weld Metal Overmatch. The effect of weld metal overmatch on Tensile Strain Capacity is highlighted in Figure 9. It can be seen that all three sets of results (ExxonMobil and CRES GMAW and SMAW/FCAW) exhibit a similar trend with tensile strain capacity increasing with weld metal overmatch. For the base case example the predicted Tensile Strain Capacity increases by approximately 0.5–0.7% for an increase in overmatch from 10–30% confirming that weld metal overmatch is extremely beneficial and can impact tensile strain capacity significantly.

Uniform Elongation (UEL). Although the CRES Tensile Strain Capacity model accounts for Uniform Elongation indirectly as a function of the tensile properties (Y/T ratio) it does not include UEL as an input variable. In comparison UEL is an input variable in the ExxonMobil Tensile Strain Capacity model. The effect of UEL on Tensile Strain Capacity is highlighted in Figure 10 for the ExxonMobil model. It can be seen that Tensile Strain Capacity increases with increasing UEL. Given that most high strength pipe materials considered for strain based design will have UELs between 6-10% the results in Figure 10 show that increasing UEL from 6% to 10% will increase the tensile strain capacity by approximately 0.50%.

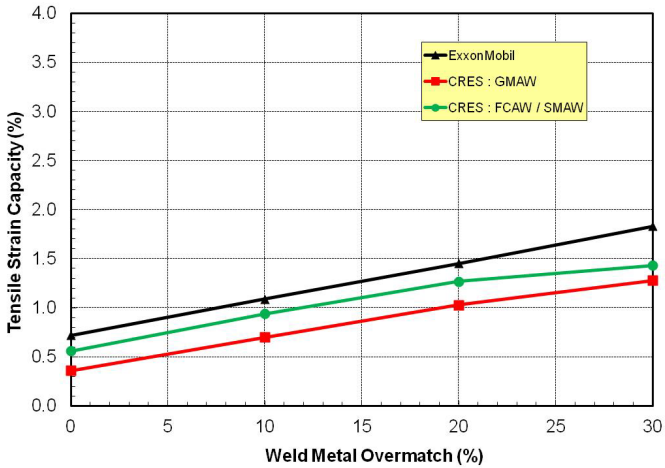


Figure 9. Effect of weld metal overmatch on tensile strain capacity.

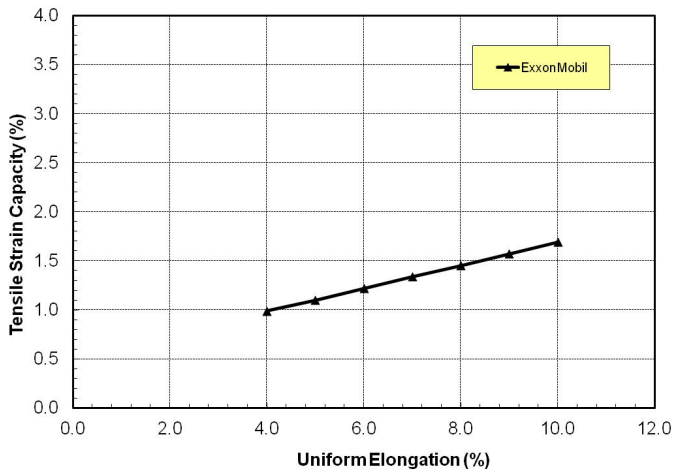


Figure 10. Effect of uniform elongation on Tensile Strain Capacity.

Hi-Lo Misalignment. Hi-Lo misalignment at a girth weld produces local through wall bending due to eccentricity. Hi-Lo misalignment can be controlled but is almost impossible to eliminate completely. Typical misalignments for cross country pipelines are in the range 2.0 – 4.0 mm although larger levels of misalignment can occur on occasion. For fatigue critical offshore pipelines Hi-Lo is frequently controlled to much tighter limits by either pipe end machining (Counter-boring) or matching and rotating pipe. The effect of Hi-Lo misalignment for the base case example is highlighted in Figure 11. All three TSC equations predict a consistent trend. It is clear that Hi-Lo misalignment can have a huge impact on tensile strain capacity. It should also be recognized that although the plot in Figure 11 extends back to zero Hi-Lo misalignment, controlling Hi-Lo misalignment in a large diameter cross country pipeline to less than 1.5 mm is probably not achievable.

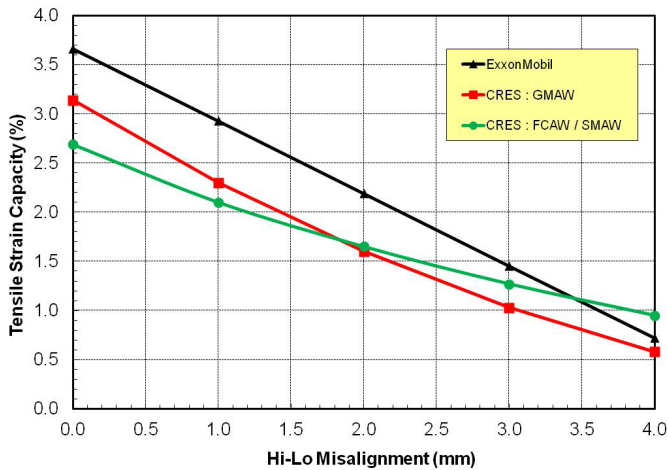


Figure 11. Effect of hi-lo misalignment on Tensile Strain Capacity.

Design Factor / Wall Thickness. The Pipeline Design Factor defines the hoop stress due to internal pressure as a percentage of the pipe material's specified minimum yield strength. Most onshore pipelines in remote locations operate at Design Factors of 72% or 80%. For more densely populated regions the Design Factor is generally reduced to 50-60%. Since most pipelines operate at a constant pressure the Design Factor is generally controlled by changing the wall thickness of the pipe. However, it is important to recognize that for a constant operating pressure a change in Design Factor results in a change in hoop stress and wall thickness both of which may impact Tensile Strain Capacity. The effect of Design Factor (assuming a constant operating pressure and varying wall thickness) on Tensile Strain Capacity is presented in Figure 12. It can be seen that all three models predict a consistent trend, i.e., the Tensile Strain Capacity increases with decreasing Design Factor (increasing wall thickness). Moreover increasing the wall thickness has a significant benefit on tensile strain capacity. Since the ExxonMobil TSC model is based on a fixed Design Factor of 80% then, for a pipeline of a constant thickness, a change in Design Factor (i.e. changing operating pressure) does not influence the predicted Tensile Strain Capacity. The CRES TSC model does include an allowance for Design Factors less than 60% but is independent of Hoop Stress between 60-80% SMYS as highlighted in Figure 13.

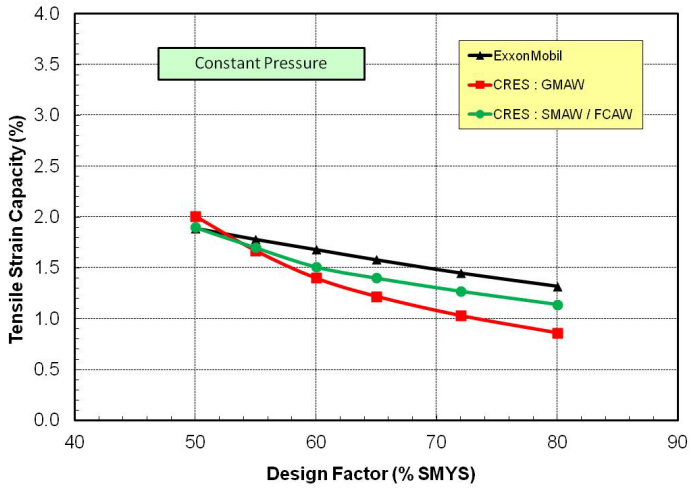


Figure 12. Effect of pipeline Design Factor on Tensile Strain Capacity (constant pressure).

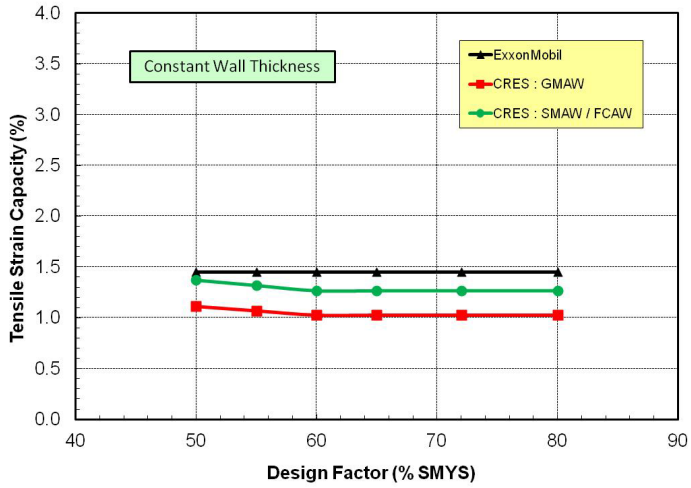


Figure 13. Effect of pipeline Design Factor on Tensile Strain Capacity (constant wall thickness).

## Discussion of Results

It is clear from the results of the sensitivity analyses that the predicted Tensile Strain Capacities obtained from the ExxonMobil and CRES Tensile Strain Capacity models are in reasonable agreement. Moreover, the sensitivity to the different input parameters is extremely similar confirming that both models capture the significance of the major input parameters on tensile strain capacity. This is encouraging and adds confidence to both models. The results also highlight that, at least for the example studied, the ExxonMobil TSC equations consistently predict slightly higher tensile strain capacities. This may, in large part, be associated with the estimation of the apparent CTOD toughness used in the CRES Model. At present the CRES model offers three methods of estimating apparent CTOD which can give rise to apparent CTOD values that differ by as much as a factor of 2. The estimation of apparent CTOD and its impact on predicted tensile strain capacity is clearly a concern, although based on the results of the sensitivity analyses the main effect may be to increase conservatism in the predicted strain capacity as opposed to yielding non-conservative predictions. Based on the results of the sensitivity analyses the option of estimating apparent CTOD that gives the closest agreement to the ExxonMobil model is the SENT R-curve approach. It should be noted however that at small crack growths R-curve data can exhibit reasonably high levels of scatter that are associated with the determination of the original crack size and hence the starting point to calculate crack growth.

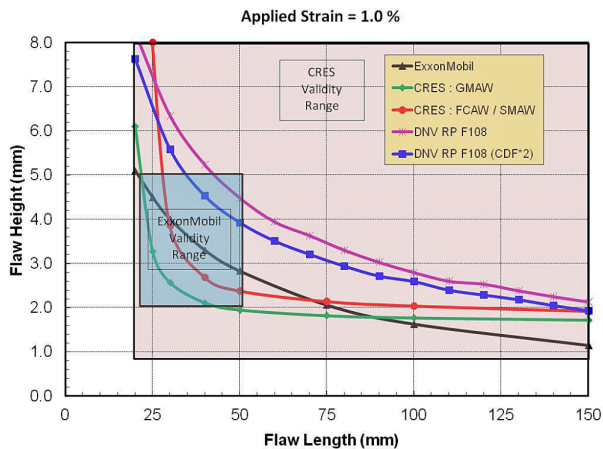
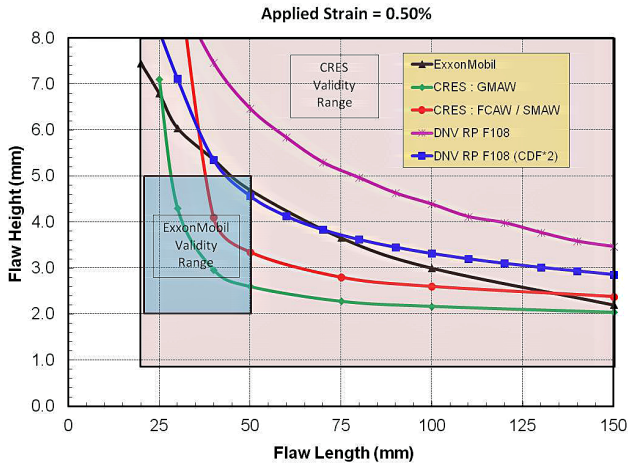
### **Comparison of ExxonMobil, CRES and DNV RP F108 Models**

#### General

In addition to the direct comparison of the ExxonMobil and CRES models a comparison was made between the ExxonMobil, CRES and DNV RP F108 models for the base case example at applied strains of 0.50%, 1.0% and 1.5%. In the case of the DNV RP F108 model analyses were performed with the predicted crack driving force multiplied by 1.0 (standard DNV RP F108) and 2.0 (simple adjustment to account for the biaxial loading effect on crack driving force). The results of the analyses are presented in Figure 14 as plots of tolerable flaw height versus tolerable flaw length. It should be noted that although the factor of 2.0 in the DNV RP F108 model takes some account for biaxial loading the DNV RP F108 model does not consider a number of other parameters that are considered in the ExxonMobil and CRES models, in particular weld metal overmatch. Also included in Figure 14 are validity boxes for the ExxonMobil (blue box) and CRES (red box) that show the validity range of flaw sizes covered by the two models. It is immediately obvious from Figure 14 that the CRES validity box is much larger than the ExxonMobil validity box which, in comparison, restricts the maximum flaw length to 50 mm.

The results in Figure 14 show that despite the fact that the DNV RP F108 model does not take into account weld overmatch the predicted flaw tolerance from DNV RP F108, even when corrected for biaxial loading, is larger than the flaw tolerance obtained from the ExxonMobil and CRES models. Moreover, the difference between the DNV predicted flaw tolerance and the ExxonMobil and CRES predicted flaw tolerances increases with increasing applied strain. The ExxonMobil and CRES results are reasonably consistent with the results of the sensitivity analyses over the validity range of the ExxonMobil model. At longer flaw lengths, the ExxonMobil predicted flaw tolerance is generally larger than the CRES predicted flaw tolerance

but as the flaw length decreases the predictions flip over with the CRES model predicting larger flaw tolerance. This is also highlighted in Figure 15 which shows the effect of flaw length on Tensile Strain Capacity for flaw heights of 3.0 and 5.0 mm in the base case example. The results in Figure 15 show that, as the flaw length decreases, the tensile strain capacity predictions for the CRES model increase more rapidly than the ExxonMobil predictions.



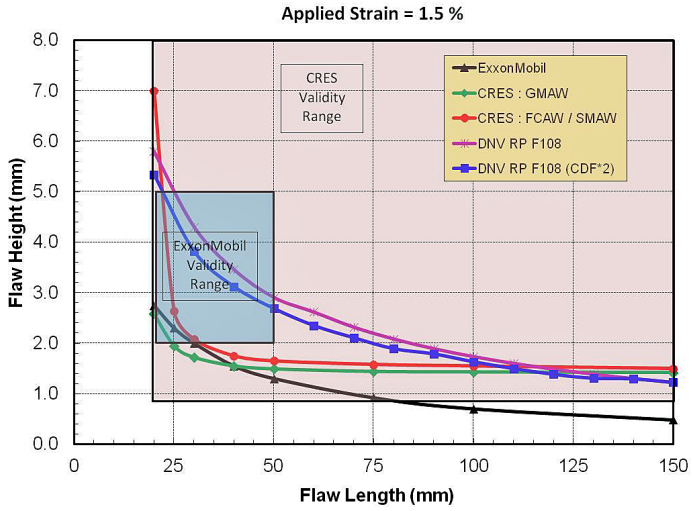


Figure 14. Comparison of ExxonMobil, CRES and DNV RP F108 models.

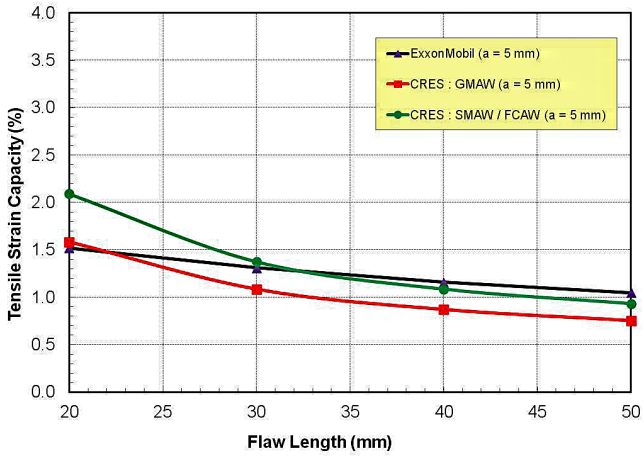


Figure 15. Effect of flaw length on Tensile Strain Capacity.

The main difference between the CRES and the ExxonMobil & DNV RP F108 predictions is at long flaw lengths where the ExxonMobil and DNV RP F108 models continue to predict decreasing flaw height with increasing flaw length as compared to the CRES model which exhibits a plateau in flaw height. It should be noted that, since the ExxonMobil model is restricted to a maximum flaw length of 50 mm it is speculative to extrapolate this model beyond the validity limit of 50 mm even though the trend from the ExxonMobil and DNV RP F108 models are consistent. Since most high strain applications in pipelines occur as a result of global bending, as opposed to global tension, the trend exhibited by the CRES model is more in line with expected behavior, i.e. as the flaw length increases there comes a point where it starts to behave as a long continuous flaw. For unusual cases where the loading is predominantly global tension this may not be the case depending on whether collapse is defined as local ligament collapse versus global or cross section collapse.

### Summary

This paper presents a comparison of the recently proposed ExxonMobil and CRES strain based ECA models and also compares the predictions from these models with the DNV RP 108 ECA procedure developed to assess pipelines installed by reeling. A series of sensitivity analyses were performed for a candidate pipeline application to compare the models and determine how predicted tensile strain capacity is influenced by key input variables. The major findings of this work can be summarized as follows:

1. In general, the predicted Tensile Strain Capacities obtained from the ExxonMobil and CRES Tensile Strain Capacity models are in reasonable agreement. Moreover, the sensitivity to the different input parameters is extremely similar confirming that both models capture the significance of the major input parameters on tensile strain capacity.
2. The major difference between the ExxonMobil and CRES models is the influence of flaw length. As flaw length decreases the CRES model predicts a more significant increase in tensile strain capacity than the ExxonMobil model. Conversely at long flaw lengths (extending beyond the 50 mm ExxonMobil validity limit) the ExxonMobil model continues to predict decreasing flaw height with increasing flaw length as compared to the CRES model which exhibits a plateau in flaw height. The validity limits of the ExxonMobil Level 2 Tensile Strain Capacity equations do not permit acceptance criteria to be developed for flaws longer than 50 mm. If flaw acceptance criteria are needed for long shallow flaws a Level 3 analysis is required.
3. The CRES Tensile Strain Capacity model is sensitive to the method of estimating apparent CTOD toughness. At present the CRES model offers three methods of estimating apparent CTOD, which can give rise to apparent CTOD toughness values and predicted strain capacities that differ by as much as a factor of 2. The estimation of apparent CTOD and its impact on predicted tensile strain capacity should be noted by end users. Apparent CTOD toughness derived from traditional Charpy and/or CTOD tests tends to produce more conservative strain capacity predictions than using apparent CTOD toughness derived from SENT tests. Based on the results of the sensitivity analyses presented in this paper the option of estimating apparent CTOD from an SENT R-curve gives the closest agreement to the ExxonMobil model.

4. The ExxonMobil and CRES models both indicate that, in addition to weld metal overmatch, control of Hi-Lo misalignment is critical for sections of pipeline that may experience high strains in operation. For pipelines where only small sections of the route have high strain demand increasing pipe wall thickness can also provide significant benefit.
5. The predicted flaw tolerance from DNV RP F108, even when corrected for biaxial loading by applying a factor of two to the crack driving force, is larger than the flaw tolerance obtained from the ExxonMobil and CRES models. Moreover, the difference between the DNV predicted flaw tolerance and the ExxonMobil and CRES predicted flaw tolerances increases with increasing applied strain. This finding is somewhat surprising since the base case example had 20% overmatching which the DNV RP F108 procedure does not consider.

### References

1. DNV RP F108 “Fracture Control for Pipeline Installation Methods Introducing Cyclic Plastic Strain,” (Det Norske Veritas, 2006).
2. D.P. Fairchild et al., “A Multi-Tiered Procedure for Engineering Critical Assessment of Strain Based Pipelines,” *Proceedings of the Twenty First International Offshore and Polar Engineering Conference 2011*, Maui, Hawaii, (June 2011).
3. Y.Y. Wang, M. Liu and Y. Song, “Second Generation Models for Strain Based Design” (Contract PR-ABD-1 – Project 2, Final Report, Pipeline Research Council International, August 2011).
4. J.R. Gordon, N. Zettlemoyer and W.C. Mohr, “Crack Driving Force in Pipelines to Large Strain and Biaxial Stress Conditions,” *Proceedings of the 17<sup>th</sup> International Offshore and Polar Engineering Conference 2007*, Lisbon, Portugal, (June 2007).
5. W. Cheng et al., “Test Methods for Characterization of Strain Capacity: Comparison of R-curves from SENT / CWP / FS Tests,” *Proceedings of Pipeline Technology Conference 2009*, Ostend, Belgium, (2009).
6. Y.Y. Wang, M. Liu and X. Long, “Validation and Documentation of Tensile Strain Limit Design Models for Pipelines” (Contract PR-ABD-1 – Project 1, Final Report, Pipeline Research Council International, August 2011).
7. BS 7910 “Guide to Methods for Assessing the Acceptability of Flaws in Metallic Structures,” 2005.
8. D.Y. Park et al., “Evaluation of Fracture Toughness of X100 Pipe using SE(B) and clamped SE(T) Single Specimens,” *Proceedings of the 8th International Pipeline Conference 2010*, Calgary, Alberta, Canada, (2010).